ACS APPLIED MATERIALS & INTERFACES

Research Article

www.acsami.org

Aqueous Solution-Deposited Molybdenum Oxide Films as an Anode Interfacial Layer for Organic Solar Cells

Qinghua Yi,[†] Pengfei Zhai,[†] Yinghui Sun,[†] Yanhui Lou,[†] Jie Zhao,[†] Baoquan Sun,[‡] Brian Patterson,[§] Hongmei Luo,[§] Wenrui Zhang,[∥] Liang Jiao,[∥] Haiyan Wang,[∥] and Guifu Zou*[,†]

[†]College of Physics, Optoelectronics, and Energy and Collaborative Innovation Center of Suzhou Nano Science and Technology, Soochow University, Suzhou 215006, People's Republic of China

[‡]Institute of Functional Nano & Soft Materials, Soochow University, Suzhou 215123, People's Republic of China

[§]Department of Chemical and Materials Engineering, New Mexico State University, Las Cruces, New Mexico 87003, United States,

[∥]Department of Electrical and Computer Engineering, Texas A & M University, College Station, Texas 77843, United States

Supporting Information

ABSTRACT: In this study, we report the growth of molybdenum oxide (MoO_x) film by polymer-assisted deposition (PAD), an environmentally friendly strategy in an aqueous system. The MoO_x film has good crystal quality and is dense and smooth. The transparency of the film is >95% in the wavelength range of 300−900 nm. The device based on P3HT:PCBM absorber material was fabricated. The solar cell with PAD-MoO_x as an anode interfacial layer exhibits great performance, even better than that of a solar cell with PEDOT:PSS or evaporated MoO_x as an anode interfacial layer. More importantly, the solar cells based on the growth of MoO_x have a longer term stability than that of solar cells based on PEDOT:PSS. These results demonstrate the aqueous PAD technology provides an alternative strategy not only for the thin films' growth of applied materials but also for the solution processing for the low-cost fabrication of future materials to be applied in the field of solar cells.

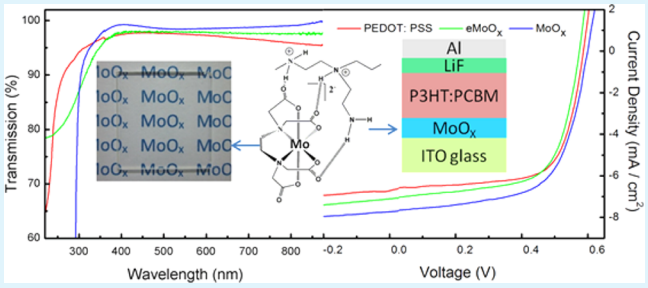

KEYWORDS: *polymer-assisted deposition, molybdenum oxide, anode interfacial layer, solar cell*

INTRODUCTION

Transition metal oxides,[1] such as molybdenum oxide,[2−4] vanadium oxide,[5] tungsten oxide,[6,7] zinc oxide,[8,9] nickel oxide,[10] germanium dioxide,[11] and so on, are emerging as important materials due to their optical and semiconducting properties. In particular, molybdenum oxide is one of the most promising materials for practical applications due to its nontoxic and cost-effective synthesis. Therefore, it is widely applied in optically switchable coating,[5,12] gas sensors,[13] electrochromic device (ECD) catalysis,[14] lithium ion batteries,[15] solar cells,[16−18] and so on. Until now, physical methods such as pulsed laser deposition,[19] electron beam evaporation,[20] radio frequency (RF) sputtering[21] and sublimation[22−25] have been explored to prepare molybdenum oxide films. Sublimation is widely used to deposit MoO_3 film, and for example, Ferroni et al. have successfully sublimated MoO_3 flakes on a porous W−Mo−O film;[22] Atuchin et al. reported high-quality α-MoO_3 single crystals have been grown by sublimation in air atmosphere.[23] Development of alternative approaches involving low-cost and large-area deposition of such films has attracted great attention. Polymer-assisted deposition (PAD) is an aqueous chemical solution method for thin film growth, which has been successfully developed to prepare single element materials,[26] metal oxides,[27] and metal carbides films.[28,29] There are several advantages for growing high-quality films. First, the polymer binds the metal ions by electrostatic attraction, hydrogen bonding, covalent bonding, or a combination thereof, and form the metal complex; meanwhile, the high molecular polymer will remove the unwanted anions or cations by filtering. Second, the precursor is environmentally friendly in aqueous systems. Third, the film prepared by PAD is dense, smooth, and uniform without visible cracks or voids.[26] In comparison with PAD, the typical sol−gel process utilizes the hydrolysis of metal alkoxide to form sol−gel and then grow the final films. On the contrary, the polymer-assisted deposition prevents the metal ion hydrolysis by combining the metal ions with polymer to form a stable precursor solution and then control the material growth in a molecular level, resulting in the high-quality film. In this study, we have utilized PAD method to grow molybdenum oxide film.

It is well-known that inserting an anode interfacial layer as hole selective layer between the anode and the active layer to minimize the hole extraction barriers is an excellent way to improve the performance of the organic solar cells. Poly(3,4-

Received: September 16, 2014
Accepted: December 23, 2014
Published: December 23, 2014

DOI: 10.1021/am506367g
ACS Appl. Mater. Interfaces 2015, 7, 18218−18224

ethylenedioxythiophene):poly(styrenesulfonate) (PEDOT:PSS) has been commonly employed as an anode interfacial layer for organic solar cells. However, the PEDOT:PSS solution corrodes the indium tin oxide (ITO) surface in the cell due to the acidic (pH = 1)[16,30] and hygroscopic nature[31] that results in deterioration of the solar cell performance. Thus, it is important to find a stable and friendly anode interfacial material to replace the PEDOT:PSS in organic solar cells. It should be noted that molybdenum oxide has good hole mobility, chemical stability, and transparency in the visible light.[16,32] According to previous reports,[17,33−36] molybdenum oxide might possess a shallow ionization potential of ∼5.3 eV and electron affinity of ∼2.2 eV, its high work function is found to pin the Femi-level of the electrode, although the value of work function is dependant on the cation oxidation state. Therefore, this material has a great potential to be used as a hole selective layer in solar cells. Until now, the solar cell based on MoO_3 hole transport layer exhibited PCEs from 2 to 4%[9,30,37] in the poly(3-hexylthiophene):phenyl-C61-butyric acid methyl ester (P3HT:PCBM) composite active layer. Herein, we have also attempted to incorporate as-grown MoO_x film into the organic solar cell: ITO/MoO_x/P3HT:PCBM/LiF/Al. The experimental results show not only that the as-grown molybdenum oxide film can be used as a semiconducting material but also that the PAD technique has great significance in solution processing of photovoltaic devices.

EXPERIMENTAL SECTION

Preparation of Molybdenum Oxide Films by PAD. To grow molybdenum oxide films, we utilized a two-step method: (1) the polyethylenimine (PEI) and ethylenediaminetetraacetic acid (EDTA) were used to bind the Mo ions and form the homogeneous polymeric precursor, and (2) the molybdenum precursor solution was spin-coated onto the (001) $LaAlO_3$ (LAO) substrate followed by annealing in air. To prepare the stable precursor of Mo, we added 2 g of ammonium molybdate ($(NH_4)_6Mo_7O_{24}{\cdot}4H_2O$) into a solution that included 2 g of EDTA and 40 mL of deionized water (DI-water), followed by the dropwise addition of 2 g of PEI in the solution. After continuous stirring for few minutes, the solution was filtered by Amicon ultrafiltration with a molecular weight of <10 000 g mol^{-1} several times. Finally, the obtained precursor solution was diluted to a concentration of 0.48 mol L^{-1}.

Device Fabrication. The device structure (ITO/MoO_x/P3HT:PCBM/LiF/Al) of the solar cell was fabricated. First, the ITO substrates were cleaned in an ultrasonic bath with acetone, alcohol, and DI-water, sequentially. The Mo precursor of various concentrations were spin-coated on cleaned ITO substrates at 4000 rpm for 30 s followed by heating at 500 °C for 10 min in air to form the MoO_x layer. The eMoO_x was thermally evaporated with a base pressure of about 1 × 10^{-6} Torr at a rate of 0.3 Å S^{1-} for 6 nm. Second, the active layer of P3HT:PCBM was spin-coated on the MoO_x layer at 700 rpm for 60 s in the glovebox and then the devices were thermally annealed at 120 °C for 12 min. Finally, the LiF (0.6 nm) and Al (100 nm) layers were evaporated onto the ITO/MoO_x/P3HT:PCBM structures of the devices.

Characterization. The concentration of Mo in the precursor solution was evaluated by inductively coupled plasma atomic emission spectrometer (PerkinElmer Optima 8000). X-ray diffraction (XRD) patterns of the films were measured by a Riguku D/MAX-2000PC diffraction system to evaluate the crystal structure and crystallographic orientation of the film. The cross-sectional microstructures of the films were analyzed by high resolution transmission electron microscopy (HRTEM, FEI Tecnai F20). Surface characteristics of molybdenum oxide films were analyzed by X-ray photoelectron spectroscopy (XPS, ESCALAB 250Xi). The transparency of the films was measured with an ultraviolet−visible (UV−vis) spectrometer (Shimadzu UV-2450). The surface morphologies of the films were analyzed by atomic force microscopy (AFM, Asylum Research MFP-3D-BIO). The electrical properties of the devices were tested by Keithley 2400 under air mass (AM) 1.5G solar irradiation at 100 mW cm^{-2} (Newport, Class AAA solar simulator, 94023A-U).

RESULTS AND DISCUSSION

The structure of the prepared molybdenum oxide film is characterized by XRD. Figure 1 shows the XRD $\theta-2\theta$ scan of

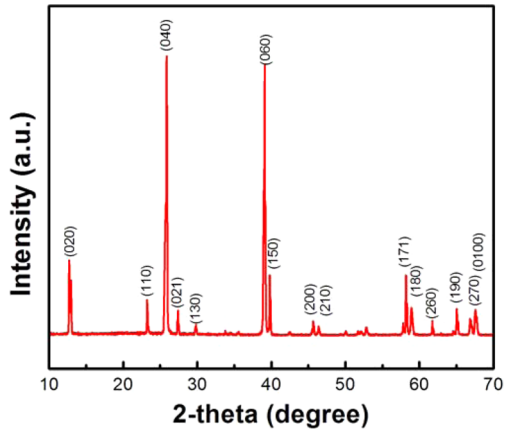

Figure 1. XRD pattern: $\theta-2\theta$ scan of molybdenum oxide film.

molybdenum oxide film. The result indicates that the film is pure phase and well-crystallized orthorhombic structure. According to the JCPDS card, the structure of the MoO_3 can be indexed to alpha-phase. In addition, the thickness of the MoO_3 is estimated to be around 30 nm by the TEM characterizations (Figures 1S). Meanwhile, the thickness of the MoO_3 film on ITO can be adjusted by the concentration of MoO_3 in the solution.

X-ray photoemission spectroscopy (XPS) was performed to analyze the surface characteristics of the molybdenum oxide films on ITO substrates, as shown in Figure 2. The Mo 3d, Mo 3p, and O 1s peaks are observed in the full scan spectra. Moreover, the intensities of the In 3d, Sn 3d, and O 1s are stronger than that from molybdenum oxide, which indicates that the molybdenum oxide film is ultrathin. Several peaks can be fitted from the spectrum of the Mo 3d core level, which corresponds to Mo^{5+} and Mo^{6+}. Meanwhile, the spectrum of O 1s shows that there is a shoulder on the higher binding energy side, implying there is more than one kind of oxygen species of O 1s. In addition, the component at 530.2 eV is attributed to crystal bulk oxygens, and the component at 531.4 eV is related to surface contamination or absorbed species.[32,38] Therefore, Mo^{5+} is attributed to the generation of O vacancies. All of the results demonstrate the presence of a major part of MoO_3.

In the present organic solar cell structure, MoO_x film plays an important role as an interfacial layer between the active layer and ITO, which is one of the effective measures to improve the PCE of solar cells. Considering premium hole extraction of molybdenum oxide, we have explored molybdenum oxide layer (MoO_x) as an interfacial layer in an organic solar cell. The schematic energy band diagram is shown in Figure 3. The polymer solar cell consists of MoO_3 as a hole injection layer, P3HT:PCBM bulk heterojunction as an active layer. Inserting an interfacial layer between the ITO and P3HT:PCBM, the potential barrier will decreases, leading to an increased

DOI: 10.1021/am506367g
ACS Appl. Mater. Interfaces 2015, 7, 18218−18224

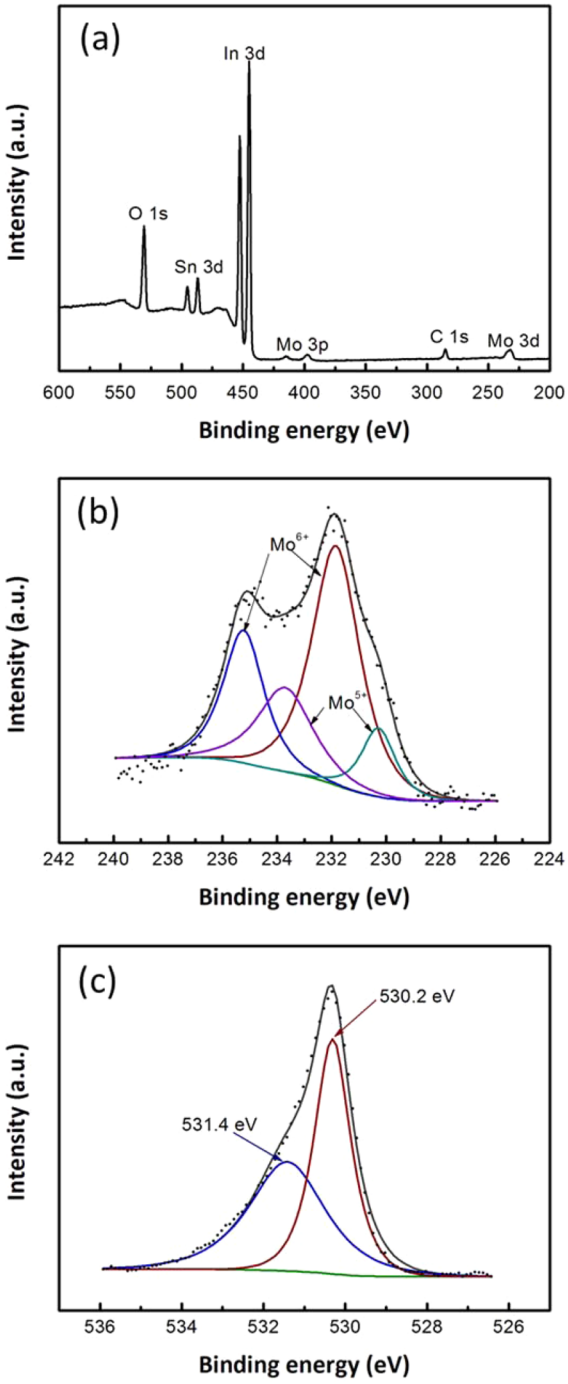

Figure 2. XPS spectra of the molybdenum oxide film on ITO substrate: (a) full scan spectra, (b) Mo 3d core level, and (c) O 1s core level.

efficiency with hole injection from P3HT to ITO. Meanwhile, lowest unoccupied molecular orbital (LUMO) of P3HT is much lower than the energy level of the conduction band (CB) of MoO_3, which significantly blocks the electron transfer to MoO_3. To investigate the influence of the PAD-MoO_x layer on the performance of photovoltaic device, we prepared the different MoO_x anode interfacial layers by adjusting concentration of Mo precursor. Figure 4 shows the current density–voltage J–V characteristics of devices under illumination from simulated AM 1.5G solar spectrum irradiation and the detailed properties are summarized in Table 1. As seen in Figure 4, the

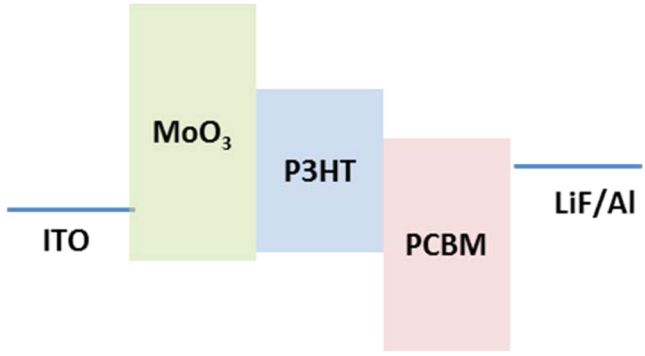

Figure 3. Schematic energy band diagram.

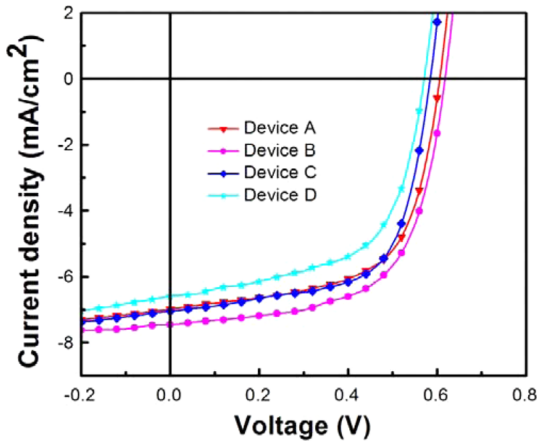

Figure 4. J–V characteristic of devices with different concentration of Mo precursor (Device A, 0.02 wt %; Device B, 0.05 wt %; Device C, 0.10 wt %; Device D, 0.25 wt %).

Table 1. Device Parameters for Conventional Architecture P3HT:PCBM Devices with Different Precursor Concentration of MoO_x Interfacial Layer

device	V_{oc} (V)	J_{sc} (mA/cm^2)	FF (%)	PCE (%)
A	0.58	7.69	60.5	2.69
B	0.60	7.60	64.6	2.94
C	0.58	7.03	64.5	2.64
D	0.57	6.58	59.5	2.23

device shows the best performance when the concentration of Mo precursor in the active layer is ~0.05 wt %. To determine the origin of the effect of different MoO_x layers on the solar cells, we used AFM to analyze the surface morphologies of the layers prepared by the different concentration of MoO_x (Figure 5). It was found that Device B, with the highest RMS 2.2 nm, has the best performance, and Device D, with the lowest RMS of 1.4 nm, has the poorest performance. Thus, it is inferred that the rougher surface of MoO_x hole selective layer somehow enhances the photovoltaic conversation efficiency. In general, the rough morphology of a film increases the interface area between the hole selective layer and active layer, and thus, it may lead to the increase of the hole collection efficiency, which was beneficial to the performance of the solar cells.[39−42] A similar phenomena have been reported in the literate.[34,43]

For comparison with the best performance MoO_x based solar cell (Device IV), we prepared reference devices with PEDOT:PSS (Device II), eMoO_x (Device III), and without any interfacial layer (Device I). Figure 6 shows the J–V

DOI: 10.1021/am506367g
ACS Appl. Mater. Interfaces 2015, 7, 18218−18224

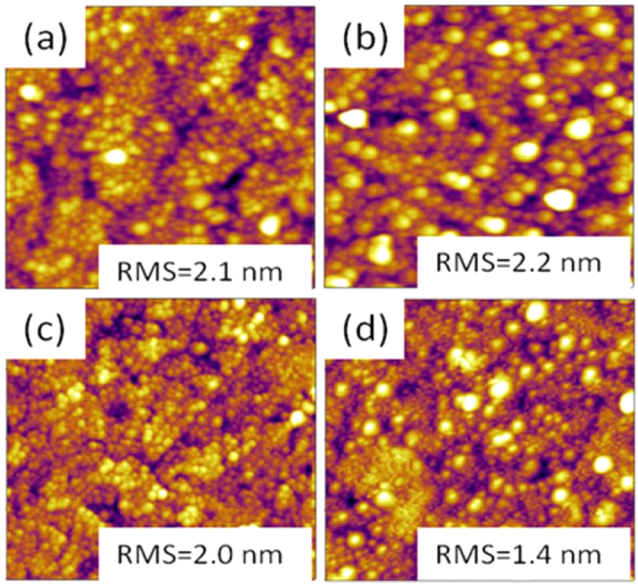

Figure 5. AFM images of MoO_x films formed on ITO substrates with different concentrations of precursor. (a) Device A, 0.02 wt %; (b) Device B, 0.05 wt %; (c) Device C, 0.10 wt %; and (d) Device D, 0.25 wt %.

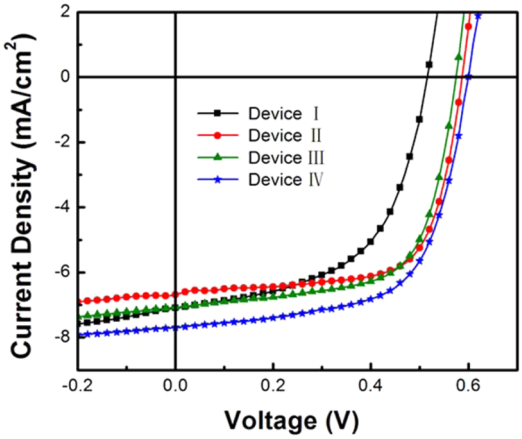

Figure 6. $J-V$ characteristic of the devices with different interfacial layers under the simulated AM1.5G spectrum illumination (Device I, ITO/P3HT:PCBM/LiF/Al; Device II, ITO/PEDOT:PSS/P3HT:PCBM/LiF/Al; Device III, ITO/thermal evaporated MoO_x($eMoO_x$)/P3HT:PCBM/LiF/Al; Device IV, ITO/MoO_x/P3HT:PCBM/LiF/Al).

characteristics of the P3HT:PCBM based devices under the simulated AM 1.5G solar spectrum illuminations. Meanwhile, the detailed properties are summarized in Table 2. As seen from the results of the photovoltaic test, the solar cell without the buffer layer (Device I) exhibits the poorer performance as compared to the solar cells with buffer layer (Devices II, III, and IV). Thus, it clearly suggests that the buffer layer between the anode and the active layer in the solar cells does improve the photovoltaic performance. Alike the reports,[44,45] the buffer layer might effectively block the recombination of hole–electron pairs in solar cells. The J_{sc} and PCE of Device IV with PAD-MoO_x are obviously higher than those of the Device II with PEDOT:PSS layer. It might be caused from the work function of MoO_x, which is higher than that of PEDOT:PSS. The MoO_x pin to the Fermi level of the contact electrode and the highest occupied molecular orbital (HOMO) of donor polymer are good for hole extracted while blocking electron transported.[45−48] Therefore, the device with MoO_x layer shows better photovoltaic parameters than the one with PEDOT:PSS layer. Further, it is worth noting in Figure 6 that performance of Device IV with PAD-MoO_x film is even better than that of the device with evaporated MoO_x layer. It is well-known that higher transparency of the window layer in solar cells corresponds to the less light loss that might result in higher performance of solar cells. To explore this in the anode interfacial layer, we investigate the optical transparency of the interfacial layers of present devices. Figure 7 shows the UV–vis transmission spectra of the PEDOT:PSS, $eMoO_x$, and PAD-MoO_x layers prepared in the similar conditions as in the devices. All of the three layers show good transparency with the optical transmission ~95% in the wavelength range of 300–900 nm. It is interesting to note that the transparency of PAD grown MoO_x film is even higher than those of the PEDOT:PSS and the $eMoO_x$ films. It can be also demonstrated by the symbol on the paper clearly observed in the inset of Figure 7. Thus, we believe that the less light loss in the present PAD grown MoO_x film is favorable for efficient harvesting of solar photons in the active layer that leads to better photovoltaic parameters (V_{oc}, J_{sc}) obtained in the Device IV with PAD-MoO_x layer.

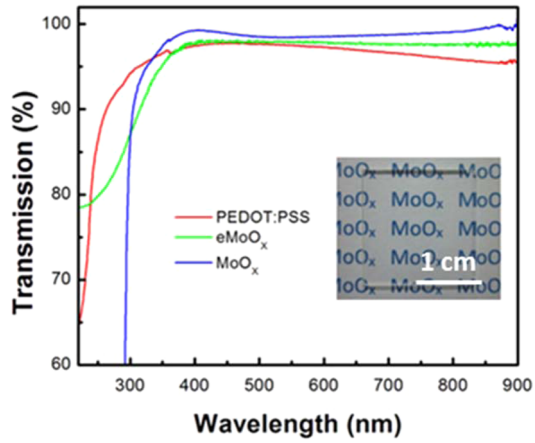

Figure 7. UV–vis transmission spectra of the MoO_x, $eMoO_x$, and PEDOT:PSS films; (inset) photograph of the MoO_x thin film on a labeled paper.

Table 2. Device Parameters of P3HT:PCBM-Based Devices with Different Interfacial Layer

device	V_{oc} (V)	J_{sc} (mA/cm^2)	FF (%)	PCE (%)
I	0.51	7.073	56.5	2.04
II	0.58	6.644	69.8	2.68
III	0.57	7.051	66.5	2.67
IV	0.60	7.60	64.6	2.94

To illustrate the stability of organic solar cell, we tested the device with PEDOT:PSS hole selective layer and PAD-MoO_x hole selective layer under continuous light-illumination in air. As Figure 8 shows, PEDOT:PSS-based devices degrade to an average value below 20% of the initial efficiency within the first 500 min under the continuous light illumination in air, while the MoO_x-based devices degrade to an average value about 60% of the initial efficiency within the first 500 min under the continuous light illumination in air. The decrease of the PCE in

DOI: 10.1021/am506367g
ACS Appl. Mater. Interfaces 2015, 7, 18218–18224

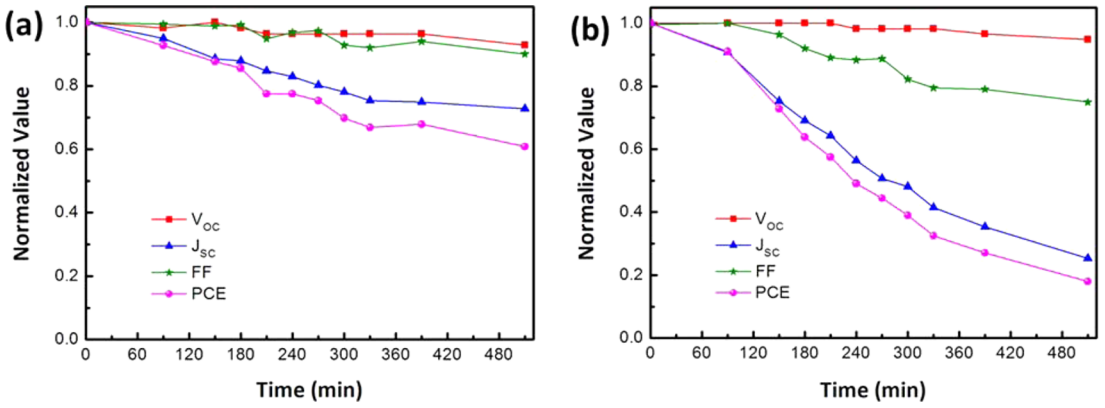

Figure 8. (a) Stabilities of key parameters in organic solar cell with MoO_x prepared by polymer-assisted deposition as a hole selective layer under continuous light-illumination in air. (b) Stabilities of key parameters in organic solar cell with conventional PEDOT:PSS as a hole selective layer under continuous light-illumination in air.

two cases is mainly attributed to a deterioration of both J_{SC} and FF.[49,50] Some researchers[51−53] report that the binding energy of the spectrum peaks will have a regular chemical shift if the chemical structure or the valence state has changed. On the basis of the XPS results shown in Figure 2a, the binding energies of In $3d^5$ and Sn $3d^5$ have not shifted, which indicates that the structure and the valence state of ITO has not changed. These can also illustrate that the MoO_3 has not reacted with ITO. Therefore, we can conclude that the MoO_x based device with a longer term stability comparable to that PEDOT:PSS-based device.

CONCLUSIONS

Molybdenum oxide (MoO_x) films prepared by polymer-assisted deposition have high crystal quality. Due to the excellent transparency (>95%) of high-quality PAD-MoO_x, the solar cell with PAD-MoO_x as an anode interfacial layer exhibits great performance, even better than that of the PEDOT:PSS or eMoO_x as an anode interfacial layer in a solar cell. Moreover, the solar cells based on the growth of MoO_x have a longer term stability than that with PEDOT:PSS. Accordingly, PAD technology provides an alternative strategy not only for film growth but also for cost-effective solution processing for future materials in the field of renewable energy.

ASSOCIATED CONTENT

Supporting Information

Cross-sectional HRTEM image and In $3d^5$ and Sn $3d^5$ XPS spectra results. This material is available free of charge via the Internet at http://pubs.acs.org.

AUTHOR INFORMATION

Corresponding Author

* E-mail: zouguifu@suda.edu.cn.

Author Contributions

The manuscript was written through contributions of all authors. All authors have given approval to the final version of the manuscript.

Notes

The authors declare no competing financial interest.

ACKNOWLEDGMENTS

We gratefully acknowledge the support from the 973 Program Special Funds for the Chief Young Scientist (2015CB358600), the Excellent Young Scholar Fund from National Natural Science Foundation of China (21422103), the Jiangsu Fund for Distinguished Young Scientist (BK20140010), the Priority Academic Program Development of Jiangsu Higher Education Institutions (PAPD), and Jiangsu Scientific and Technological Innovation Team (2013). The TEM work at Texas A&M University was funded by the U.S. National Science Foundation (NSF-0846504). H.L. thanks New Mexico EPSCoR for funding support (NSF-1301346).

REFERENCES

(1) Meyer, J.; Hamwi, S.; Kröger, M.; Kowalsky, W.; Riedl, T.; Kahn, A. Transition Metal Oxides for Organic Electronic: Energetics, Device Physics, and Applications. *Adv. Mater.* **2012**, *24*, 5408−5427.

(2) Bernede, J. C.; Cattin, L.; Morsli, M. About MoO_3 as Buffer Layer in Organic Optoelectronic Devices. *Technol. Lett.* **2014**, *1*, 5−17.

(3) Tian, B.; Ban, D.; Aziz, H. Enhanced Bulk Conductivity and Bipolar Transport in Mixtures of MoO_x and Organic Hole Transport Materials. *Thin Solid Films* **2013**, *536*, 202−205.

(4) Irfan; Ding, H.; Gao, Y.; Kim, D. Y.; Subbiah, J.; So, F. Energy Level Evolution of Molybdenum Trioxide Interlayer between Indium Tin Oxide and Organic Semiconductor. *Appl. Phys. Lett.* **2010**, *96*, 073304.

(5) Shrotriya, V.; Li, G.; Yao, Y.; Chu, C. W.; Yang, Y. Transition Metal Oxides as the Buffer Layer for Polymer Photovoltaic Cells. *Appl. Phys. Lett.* **2006**, *88*, 073508.

(6) Han, S.; Shin, W. S.; Seo, M.; Gupta, D.; Moon, S. J.; Yoo, S. Improving Performance of Organic Solar Cells Using Amorphous Tungsten Oxides as an Interfacial Buffer Layer on Transparent Anodes. *Org. Electron.* **2009**, *10*, 791−797.

(7) Tao, C.; Ruan, S.; Xie, G.; Kong, X.; Shen, L.; Meng, F.; Liu, C.; Zhang, X.; Dong, W.; Chen, W. Role of Tungsten Oxide in Inverted Polymer Solar Cells. *Appl. Phys. Lett.* **2009**, *94*, 043311.

(8) Waldo, J. E.; Beek, M.; Wienk, M.; Janssen, R. A. J. Efficient Hybrid Solar Cells from Zinc Oxide Nanoparticles and a Conjugated Polymer. *Adv. Mater.* **2004**, *16*, 109−113.

(9) Hoye, R. Z.; Muñoz-Rojas, D.; Iza, D. C.; Musselman, K. P.; MacManus-Driscoll, J. L. High Performance Inverted Bulk Heterojunction Solar Cells by Incorporation of Dense, Thin ZnO Layers Made Using Atmospheric Atomic Layer Deposition. *Sol. Energy Mater. Sol. Cells.* **2013**, *116*, 197−202.

(10) Steirer, K. X.; Ndione, P. F.; Widjonarko, N. E.; Lloyd, M. T.; Meyer, J.; Ratcliff, E. L.; Kahn, A.; Armstrong, N. R.; Curtis, C. J.; Ginley, D. S.; Berry, J. J.; Olson, D. C. Enhanced Efficiency in Plastic Solar Cells via Energy Matched Solution Processed NiO_x Interlayers. *Adv. Energy Mater.* **2011**, *1*, 813−820.

(11) Xu, M. F.; Shi, X. B.; Jin, Z. M.; Zu, F. S.; Liu, Y.; Zhang, L.; Wang, Z. K.; Liao, L. S. Aqueous Solution-Processed GeO_2: An Anode

DOI: 10.1021/am506367g
ACS Appl. Mater. Interfaces 2015, 7, 18218−18224

Interfacial Layer for High Performance and Air-Stable Organic Solar Cells. *ACS Appl. Mater. Interfaces* **2013**, *5*, 10866−10873.
(12) Colton, R. J.; Guman, A. M.; Rabalais, J. W. Electrochromism in Some Thin Film Transition Metal Oxides Characterized by X-ray Electron Spectroscopy. *J. Appl. Phys.* **1978**, *49*, 409.
(13) Mohamed, S. H.; Kappertz, O.; Ngaruiya, J. M.; Leervad Pedersen, T. P.; Drese, R.; Wuttig, M. Correlation between Structure, Stress, and Optical Properties in Direct Current Sputtered Molybdenum Oxide Films. *Thin Solid Films* **2003**, *429*, 135−143.
(14) Zhang, W.; Desikan, A.; Oyama, S. T. Effect of Support in Ethanol Oxidation on Molybdenum Oxide. *J. Phys. Chem.* **1995**, *99*, 14468−14476.
(15) Wang, G.; Ni, J.; Wang, H.; Gao, L. High-Performance CNT-Wired MoO_3 Nanobelts for Li-Storage Application. *J. Mater. Chem. A* **2013**, *1*, 4112−4118.
(16) Balendhran, S.; Deng, J.; Ou, J. Z.; Walia, S.; Scott, J.; Tang, J.; Wang, K. L.; Field, M. R.; Russo, S.; Zhuiykov, S.; Strano, M. S.; Medhekar, N.; Sriram, S.; Bhaskaran, M.; Kalantarzadeh, K. Enhanced Charge Carrier Mobility in Two-Dimensional High Dielectric Molybdenum Oxide. *Adv. Mater.* **2013**, *25*, 109−114.
(17) Sun, Y.; Takacs, C. J.; Cowan, S. R.; Seo, J. H.; Gong, X.; Roy, A.; Heeger, A. J. Efficient, Air-Stable Bulk Heterojunction Polymer Solar Cells using MoO_x as the Anode Interfacial Layer. *Adv. Mater.* **2011**, *23*, 2226−2230.
(18) Meyer, J.; Khalandovsky, R.; Gorrn, P.; Kahn, A. MoO_3 Films Spin-coated from a Nanoparticle Suspension for Efficient Hole-injection in Organic Electronics. *Adv. Mater.* **2011**, *23*, 70−73.
(19) Bhosle, V.; Tiwari, A.; Narayan, J. Epitaxial Growth and Properties of MoO_x ($2 < x < 2.75$) Films. *J. Appl. Phys.* **2005**, *97*, 083539.
(20) Lin, S. Y.; Chen, Y. C.; Wang, C. M.; Hsieh, P. T.; Shih, S. C. Post-annealing Effect upon Optical Properties of Electron Beam Evaporated Molybdenum Oxide Thin Films. *Appl. Surf. Sci.* **2009**, *255*, 3868−3874.
(21) Elangovan, E.; Martins, R.; Fortunato, E. Indium Molybdenum Oxide Thin Films: A Comparative Study by Two Different RF Sputtering Systems. *Phys. Status Solidi A* **2009**, *206*, 2123−2127.
(22) Ferroni, M.; Guidi, V.; Comini, E.; Sberveglieri, G.; Vomiero, A.; DellaMea, G.; Martinelli, G. Selective Sublimation Processing of a Molybdenum−Tungsten Mixed Oxide Thin Film. *J. Vac. Sci. Technol. B* **2003**, *21*, 1442.
(23) Atuchin, V. V.; Gavrilova, T. A.; Grigorieva, T. I.; Kuratieva, N. V.; Okotrub, K. A.; Pervukhina, N. V.; Surovtsev, N. V. Sublimation Growth and Vibrational Microspectrometry of α-MoO_3 Single Crystals. *J. Cryst. Growth* **2011**, *318*, 987−990.
(24) Subbiah, J.; Amb, C. M.; Irfan, I.; Gao, Y.; Reynolds, J. R.; So, F. High-Efficiency Inverted Polymer Solar Cells with Double Interlayer. *ACS Appl. Mater. Interfaces* **2012**, *4*, 866−870.
(25) Kyaw, A. K. K.; Sun, X. W.; Jiang, C. Y.; Lo, G. Q.; Zhao, D. W.; Kwong, D. L. An Inverted Organic Solar Cell Employing a Sol−Gel Derived ZnO Electron Selective Layer and Thermal Evaporated MoO_3 Hole Selective Layer. *Appl. Phys. Lett.* **2008**, *93*, 221107.
(26) Zou, G.; Luo, H.; Ronning, F.; Sun, B.; McCleskey, T. M.; Burrell, A. K.; Bauer, E.; Jia, Q. X. Facile Chemical Solution Deposition of High-Mobility Epitaxial Germanium Films on Silicon. *Angew. Chem., Int. Ed.* **2010**, *49*, 1782−1785.
(27) Jia, Q. X.; McCleskey, T. M.; Burrell, A. K.; Lin, Y.; Collis, G. E.; Wang, H.; Li, A. D.; Foltyn, S. R. Polymer-Assisted Deposition of Metal−Oxide Films. *Nat. Mater.* **2004**, *3*, 529−532.
(28) Zou, G.; Luo, H.; Zhang, Y.; Xiong, J.; Wei, Q.; Zhuo, M.; Zhai, J.; Wang, H.; Williams, D.; Li, N.; Bauer, E.; Zhang, X.; McCleskey, T. M.; Li, Y.; Burrell, A. K.; Jia, Q. X. A Chemical Solution Approach for Superconducting and Hard Epitaxial NbC Film. *Chem. Commun.* **2010**, *46*, 7837−7839.
(29) Zou, G.; Luo, H.; Baily, S.; Zhang, Y.; Haberkorn, N.; Xiong, J.; Bauer, E.; McCleskey, T.; Burrell, A.; Civale, L.; Zhu, Y.; Manus-Driscoll, J.; Jia, Q. X. Highly Aligned Carbon Nanotube Forests Coated by Superconducting NbC. *Nat. Commun.* **2011**, *2*, 428.
(30) Seiichiro, M.; Yang, Y. Solution Processed MoO_3 Interfacial Layer for Organic Photovoltaics Prepared by a Facile Synthesis Method. *Adv. Mater.* **2012**, *24*, 2459−2462.
(31) Voroshazi, E.; Verreet, B.; Buri, A.; Müller, R. D.; Nuzzo, D.; Heremans, P. Influence of Cathode Oxidation via the Hole Extraction Layer in Polymer: Fullerene Solar Cells. *Org. Electron.* **2011**, *12*, 736−744.
(32) Yang, T.; Wang, M.; Cao, Y.; Huang, F.; Huang, L.; Peng, J.; Gong, X.; Cheng, S. Z. D.; Cao, Y. Polymer Solar Cells with a Low-Temperature-Annealed Sol−Gel-Derived MoO_x Film as a Hole Extraction Layer. *Adv. Energy Mater.* **2012**, *2*, 523−527.
(33) Bolink, H. J.; Coronado, E.; Orozco, J.; Sessolo, M. Efficient Polymer Light-Emitting Diode Using Air-Stable Metal Oxides as Electrodes. *Adv. Mater.* **2009**, *21*, 79−82.
(34) Greiner, M. T.; Chai, L.; Helander, M. G.; Tang, W. M.; Lu, Z. H. Transition Metal Oxides Work Functions: The Influence of Cation Oxidation State and Oxygen Vacancies. *Adv. Funct. Mater.* **2012**, *22*, 4557−4568.
(35) Irfan; Ding, H. J.; Gao, Y. L.; Small, C.; Kim, D. Y.; Subbiah, J.; So, F. Energy Level Evolution of Air and Oxygen Exposed Molybdenum Trioxide Films. *Appl. Phys. Lett.* **2010**, *96*, 243307.
(36) Brown, P. R.; Lunt, R. R.; Zhao, N.; Osedach, T. P.; Wanger, D. D.; Chang, L. Y.; Bawendi, M. G.; Bulovic, V. Improved Current Extraction from ZnO/PbS Quantum Dot Heterojunction Photovoltaics Using a MoO_3 Interfacial Layer. *Nano Lett.* **2011**, *11*, 2955−2961.
(37) Hammond, S. R.; Meyer, J.; Widjonarko, N. E.; Ndione, P. F.; Sigdel, A. K.; Garcia, A.; Miedaner, A.; Lloyd, M. T.; Kahn, A.; Ginley, D. S.; Berry, J. J.; Olson, D. Low-Temperature, Solution-Processed Molybdenum Oxide Hole-Collection Layer for Organic Photovoltaics. *J. Mater. Chem.* **2012**, *22*, 3249−3254.
(38) Ramana, C. V.; Atuchin, V. V.; Kesler, V. G.; Kochubey, V. A.; Pokrovsky, L. D.; Shutthanandan, V.; Becker, U.; Ewing, R. C. Growth and Surface Characterization of Sputter-Deposited Molybdenum Oxide Thin Films. *Appl. Surf. Sci.* **2007**, *253*, 5368−5374.
(39) Liang, Z.; Zhang, Q.; Wiranwetchayan, O.; Xi, J.; Yang, Z.; Park, K.; Li, C.; Cao, G. Effects of the Morphology of a ZnO Buffer Layer on the Photovoltaic Performance of Inverted Polymer Solar Cells. *Adv. Funct. Mater.* **2012**, *22*, 2194−2201.
(40) Hu, J.; Wu, Z.; Wei, H.; Song, T.; Sun, B. Effects of ZnO Fabricating Process on the Performance of Inverted Organic Solar Cells. *Org. Electron.* **2012**, *13*, 1171−1177.
(41) Lee, Y. I.; Youn, J. H.; Ryu, M. S.; Kim, J.; Moon, H. T.; Jang, J. Highly Efficient Inverted Poly(3-hexylthiophene): Methano-fullerene [6,6]-Phenyl C71-Butyric Acid Methyl Ester Bulk Heterojunction Solar Cell with Cs_2CO_3 and MoO_3. *Org. Electron.* **2011**, *12*, 353−357.
(42) Zhao, D. W.; Tan, S. T.; Ke, L.; Liu, P.; Kyaw, A. K. K.; Sun, X. W.; Lo, G. Q.; Kwong, D. L. Optimization of an Inverted Organic Solar Cell. *Sol. Energy Mater. Sol. Cells* **2010**, *94*, 985−991.
(43) Xu, M. F.; Cui, L. S.; Zhu, X. Z.; Gao, C. H.; Shi, X. B.; Jin, Z. M.; Wang, Z. K.; Liao, L. S. Aqueous Solution-Processed MoO_3 as an Effective Interfacial Layer in Polymer/Fullerene based Organic Solar Cells. *Org. Electron.* **2013**, *14*, 657−664.
(44) Liu, F.; Shao, S.; Guo, X.; Zhao, Y.; Xie, Z. Efficient Polymer Photovoltaic Cells Using Solution-Processed MoO_3 as Anode Buffer Layer. *Sol. Energy Mater. Sol. Cells* **2010**, *94*, 842−845.
(45) Wong, K. H.; Ananthanarayanan, K.; Luther, J.; Balaya, P. Origin of Hole Selectivity and the Role of Defects in Low-Temperature Solution-Processed Molybdenum Oxide Interfacial Layer for Organic Solar Cells. *J. Phys. Chem. C* **2012**, *116*, 16346−16351.
(46) Matsushima, T.; Jin, G. H.; Kanai, Y.; Yokota, T.; Kitada, S.; Kishi, T.; Murata, H. Interfacial Charge Transfer and Charge Generation in Organic Electronic Devices. *Org. Electron.* **2011**, *12*, 520−528.
(47) Bernède, J. C.; Houari, S.; Nguyen, D.; Jouan, P. Y.; Khelil, A.; Mokrani, A.; Cattin, L.; Predeep, P. XPS Study of The Band Alignment at ITO/Oxide (n-Type MoO_3 or p-Type NiO) Interface. *Phys. Status Solidi A* **2012**, *209*, 1291−1297.

DOI: 10.1021/am506367g
ACS Appl. Mater. Interfaces 2015, 7, 18218−18224

(48) Lee, H.; Cho, S. W.; Han, K.; Jeon, P. E.; Whang, C. N.; Jeong, K.; Cho, K.; Yi, Y. The Origin of The Hole Injection Improvements at Indium Tin Oxide/Molybdenum Trioxide/*N*,*N*′-bis(1-naphthyl)-*N*,*N*′-diphenyl-1,1′-biphenyl-4,4′-diamine Interfaces. *Appl. Phys. Lett.* **2008**, *93*, 043308.
(49) Zilberberg, K.; Trost, S.; Schmidt, H.; Riedl, T. Solution Processed Vanadium Pentoxide as Charge Extraction Layer for Organic Solar Cells. *Adv. Energy Mater.* **2011**, *1*, 377−381.
(50) Kawano, K.; Pacios, R.; Poplavskyy, D.; Nelson, J.; Bradley, D. D. C.; Durrant, J. R. Degradation of Organic Solar Cells due to Air Exposure. *Sol. Energy Mater. Solar Cells* **2006**, *90*, 3520−3530.
(51) McIntyre, N. S.; Zetaruk, D. G. X-ray Photoelectron Spectroscopic Studies of Iron Oxides. *Anal. Chem.* **1977**, *49*, 1521−1529.
(52) Xie, Y. M.; Sherwood, P. M. A. X-ray Photoelectron Spectroscopic Studies of Carbon Fiber Surfaces. Differences in the Surface Chemistry and Bulk Structure of Different Carbon Fibers Based on Poly(acrylonitrile) and Pitch and Comparison with Various Graphite Samples. *Chem. Mater.* **1990**, *2*, 293−299.
(53) Pfluger, P.; Street, G. B. Chemical, Electronic and Structural Properties of Conducting Heterocyclic Polymers: A View by XPS. *J. Chem. Phys.* **1984**, *80*, 544−553.

DOI: 10.1021/am506367g
ACS Appl. Mater. Interfaces 2015, 7, 18218−18224